

Metazoan zooplankton in the Bay of Biscay: 16 years of individual sizes and abundances combining ZooScan and ZooCAM imaging systems.

Authors

Grandremy Nina^{1*}, Bourriau Paul¹, Daché Edwin², Danielou Marie-Madeleine³, Doray Mathieu¹, Dupuy Christine⁴, Forest Bertrand⁵, Jalabert Laetitia⁶, Huret Martin⁷, Le Mestre Sophie⁷, Nowaczyk Antoine⁸, Petitgas Pierre⁹, Pineau Philippe⁴, Rouxel Justin¹⁰, Tardivel Morgan¹⁰, Romagnan Jean-Baptiste^{1*}.

Correspondence

grandremy.n@gmail.com, jean.baptiste.romagnan@ifremer.fr

Affiliations

¹ DECOD (Ecosystem Dynamics and Sustainability), IFREMER, INRAE, Institut Agro, Nantes, Centre Atlantique - Rue de l'Île d'Yeu - BP 21105 - 44311 Nantes Cedex 03, France.

² Unité Biologie et Ecologie des Ecosystèmes marins Profonds, Laboratoire Environnement Profond, Ifremer Centre Bretagne - ZI de la Pointe du Diable - CS 10070 - 29280 Plouzané, France.

³ Unité DYNECO-PELAGOS, Laboratoire d'Ecologie Pélagique, Ifremer Centre Bretagne - ZI de la Pointe du Diable - CS 10070 - 29280 Plouzané, France.

⁴ BIOFEEL, UMRi LIENSs, La Rochelle University / CNRS, 2, rue Olympe de Gouges, 17000 La Rochelle, France.

⁵ Laboratoire Hydrodynamique Marine, Unité RDT, Ifremer Centre Bretagne - ZI de la Pointe du Diable - CS 10070 - 29280 Plouzané, France.

⁶ Sorbonne Université, Institut de la Mer de Villefranche, 06230 Villefranche-sur-mer, France.

⁷ DECOD (Ecosystem Dynamics and Sustainability), IFREMER, INRAE, Institut Agro, Centre Bretagne - ZI de la Pointe du Diable - CS 10070 - 29280 Plouzané, France.

⁸ UMR CNRS 5805 EPOC – OASU, Station Marine d'Arcachon, Université de Bordeaux, 2 Rue du Professeur Jolyet, 33120 Arcachon, France.

⁹ Département Ressources Biologiques et Environnement, Ifremer Centre Atlantique - Rue de l'Île d'Yeu - BP 21105 - 44311 Nantes Cedex 03, France.

¹⁰ Laboratoire Détection, Capteurs et Mesures, Unité RDT, Ifremer Centre Bretagne - ZI de la Pointe du Diable - CS 10070 - 29280 Plouzané, France.

* These authors contributed equally to this work.

32 **Abstract**

33 This paper presents two metazoan zooplankton datasets obtained by imaging samples collected on the Bay of
34 Biscay continental shelf in spring during the PELGAS integrated surveys, over the 2004-2019 period. The samples
35 were collected at night, with a WP2 200 μm mesh size fitted with a Hydrobios (back-run stop) mechanical
36 flowmeter, hauled vertically from the sea floor to the surface with a maximum depth set at 100 m when the
37 bathymetry is deeper. The first dataset originates from samples collected from 2004 to 2016, imaged on land with
38 the ZooScan and is composed of 1,153,507 imaged and measured objects. The second dataset originates from
39 samples collected from 2016 to 2019, imaged on board the R/V *Thalassa* with the ZooCAM and is composed of
40 702,111 imaged and measured objects. The imaged objects are composed of zooplankton individuals, zooplankton
41 pieces, non-living particles and imaging artefacts, ranging from 300 μm to 3.39 mm Equivalent Spherical
42 Diameter, individually imaged, measured and identified. Each imaged object is geolocated, associated to a station,
43 a survey, a year and other metadata. Each object is described by a set of morphological and grey level based
44 features (8 bits encoding, 0 = black, 255 = white), including size, automatically extracted on each individual image.
45 Each object was taxonomically identified using the web based application Ecotaxa with built-in, random forest
46 and CNN based, semi-automatic sorting tools followed by expert validation or correction. The objects were sorted
47 in 172 taxonomic and morphological groups. Each dataset features a table combining metadata and data, at the
48 individual object granularity, from which one can easily derive quantitative population and communities
49 descriptors such as abundances, mean sizes, biovolumes, biomasses, and size structure. Each object's individual
50 image is provided along with the data. These two datasets can be used combined together for ecological studies as
51 the two instruments are interoperable, or as training sets for ZooScan and ZooCAM users. The data presented here
52 are available in the SEANOE dataportal: <https://doi.org/10.17882/94052> (ZooScan dataset, Grandremy et al.,
53 2023c) and <https://doi.org/10.17882/94040> (ZooCAM dataset, Grandremy et al., 2023d).

54 **Keywords**

55 Zooplankton, ZooCAM, ZooScan, Bay of Biscay, imaging, PELGAS surveys.

56

57 **1 Introduction**

58 Metazoan planktonic organisms, hereafter referred to as zooplankton, encompass an immense diversity
59 of life forms, which have successfully colonized the entire ocean, from eutrophic estuarine shallow areas to
60 oligotrophic open ocean, from sunlit ocean to hadal depth. Their body sizes span five to six orders of magnitude
61 in length, from μm to tens of meters (Sieburth & Smetacek, 1978). Zooplankton plays a pivotal role in marine
62 ecosystem (Banse, 1995). It transfers the organic matter produced in the epipelagic domain by photosynthesis to
63 the deeper layers of the ocean (Siegel et al., 2016), by producing fast sinking aggregates (Turner, 2015), and by
64 diel vertical migration (Steinberg et al., 2000; Ohman & Romagnan, 2016). Zooplankton therefore participates in
65 mitigating the anthropogenic carbon dioxide build up in the atmosphere responsible for climate change. Moreover,
66 zooplankton is an exclusive trophic resource for commercially important fish during their larval stage, where a
67 shift in zooplankton species or phenology can have dramatic effects on recruitment (i.e. North Sea cod, Beaugrand
68 et al., 2003). In addition, it is a major trophic resource for adult planktivorous small pelagic fish, known as forage
69 fishes (Van der Lingen, 2006). Recent studies suggest that zooplankton dynamics may have a significant effect on
70 small pelagic fish population dynamics and individual body condition (Brosset et al., 2016; Menu et al., 2023),
71 and therefore impact wasp-waist ecosystem based fisheries and fisheries dependent socio-ecosystems, worldwide
72 (Cury et al., 2000).

73 Despite zooplankton being of such global importance in both climate change effects on ecosystems and
74 management of fisheries (Chiba et al., 2018; Lombard et al., 2019), it is still technically difficult to monitor, with
75 respect to other marine ecological compartments. Zooplankton biomass, diversity and spatio-temporal
76 distributions cannot be estimated from spaceborne sensors as phytoplankton's does (Uitz et al., 2010), and
77 zooplankton commercial exploitation data do not exist yet, as fish data does. One noticeable exception is the CPR
78 surveys network that enables zooplankton data generation at spatio-temporal scales resolved enough to study
79 climate change and diversity related zooplanktonic processes (Batten et al., 2019). Yet, generating zooplankton
80 data often requires dedicated surveys at sea, specific sampling instruments and trained taxonomic analysts.
81 Moreover, besides actual observation, modelling zooplankton remains a challenging task due to the diversity of
82 traits such as life forms, life cycles, body sizes and physiological processes exhibited by zooplankton (Mitra &
83 Davis 2010; Mitra et al., 2014). However, over the past two decades the development of imaging and associated
84 machine learning semi-automatic identification tools (Irisson et al., 2022) have greatly improved the capability of
85 scientists to analyse long (Feuilloley et al., 2022), high frequency (Romagnan et al., 2016), or spatially resolved
86 (Grandremy et al., 2023a) zooplankton time series, as well as trait based data (Orenstein et al., 2022). Imaging and
87 machine learning have particularly enabled the increased development of combined size and taxonomy
88 zooplankton ecological studies (i.e. Vandromme et al., 2014; Romagnan et al., 2016; Benedetti et al., 2019). Yet,
89 use of these machine learning tools is not trivial because these require abundant, scientifically qualified, sensor
90 specific, training image data (i.e. learning set and test set, Irisson et al., 2022), and complex hardware and software
91 setups (Panaiotis et al., 2022). One good example of such image dataset is the ZooScanNet dataset (Elineau et al.,
92 2018), which features an extensive ZooScan (Gorsky et al., 2010) imaging dataset usable as a training set for
93 ecologists as well as for imaging and machine learning scientists.

94 The objective of this paper is to present two freely available zooplankton imaging datasets, originating
95 from two different instruments, the ZooScan (Gorsky et al., 2010), and the ZooCAM (Colas et al., 2018). These

96 datasets originate from the PELGAS integrated survey in the Bay of Biscay (Doray et al., 2018a), a continental
97 shelf ecosystem supporting major European fisheries (ICES, 2021). Combined together, these datasets make up a
98 16-years time series of sized and taxonomically resolved zooplankton, along with context metadata allowing the
99 calculation of quantitative data, covering the whole Bay of Biscay continental shelf, from the French coast to the
100 continental slope, and from the Basque country to southern Brittany, in spring. These datasets can be used for
101 ecological studies (Grandremy et al., 2023a), machine learning studies, and modelling studies.

102 **2 Methods**

103 **2.1 Sampling**

104 Zooplankton samples were collected during the successive PELGAS (PELagique GAScogne) integrated
105 surveys carried out over the Bay of Biscay (BoB) French continental shelf, every year in spring from 2004 to 2019
106 on board the R/V *Thalassa*. The aim of this survey is to assess small pelagic fish biomass and monitor the pelagic
107 ecosystem to inform ecosystem based fisheries management. Fish data, hydrology, phyto- and zoo-plankton
108 samples and megafauna sightings (marine mammals and seabirds) are concomitantly collected to build long-term
109 spatially resolved time series of the BoB pelagic ecosystem. The PELGAS sampling protocols combine day-time
110 en-route data collection (small pelagic fish and megafauna), with night-time, depth integrated hydrology and
111 plankton sampling at fixed points. Detailed PELGAS survey protocols can be found in Doray et al. (2018a) and
112 Doray et al. (2021). The PELGAS survey datasets providing hydrological, primary producers, fish and megafauna
113 data are available as gridded data in the SEANOE dataportal (Doray et al., 2018b) under the following link:
114 <https://www.seanoe.org/data/00422/53389/>.

115 The number of zooplankton samples across years varied between 41 (2005) and 64 (2019), due to
116 adjustments in the sampling strategy and weather conditions, for 889 zooplankton samples collected in total. From
117 2004 to 2006, samples were collected in the southern Bay of Biscay until the Loire estuary only (Fig. 1). Sampling
118 was carried out in vertical tows during night time using a 200- μ m mesh size WP2 net, generally from 100 m depth
119 (or 5 m above the seabed) to the surface. In 2004 and 2005, the targeted maximum sampling depth was 200 m. In
120 2004, fifteen samples were collected deeper than 100 m, among which eleven were deeper than 120 m; in 2005,
121 twenty samples were collected deeper than 100 m, among which thirteen were deeper than 120 m. Before 2014,
122 the sampled water volume was estimated by multiplying the cable length by the net opening surface (0.25 m²)
123 whereas since 2014, the net was equipped with a Hydrobios back-run stop flowmeter. The samples originating
124 from 2004 to 2016 surveys were preserved in 4% formaldehyde (final concentration) and analysed on land in the
125 laboratory with the ZooScan, while since 2016 they were analysed live on board with the ZooCAM.

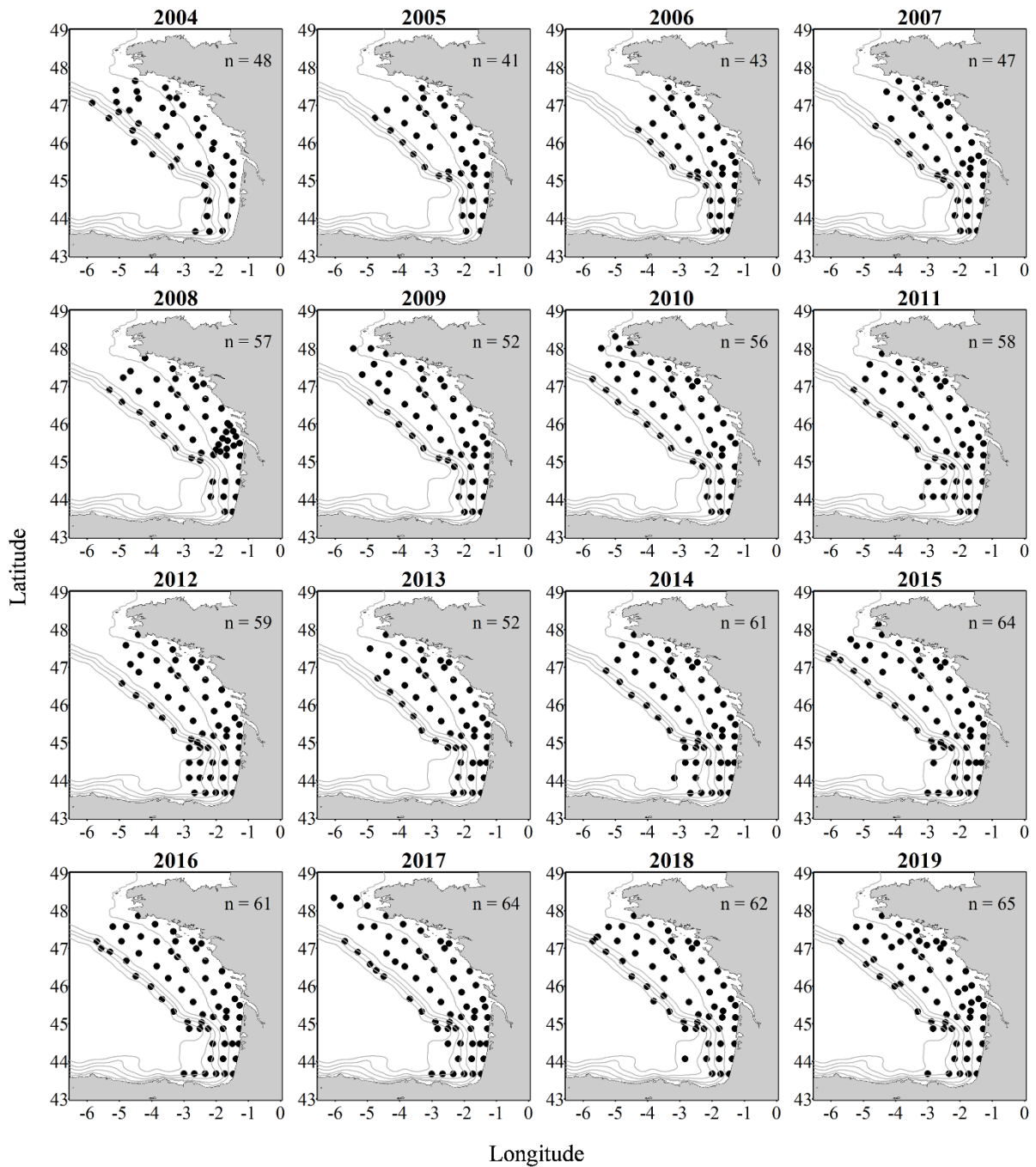
126 **2.2 Sample processing and analyses**

127 **2.2.1 Digitization with the ZooScan**

128 Preserved samples were digitized with the ZooScan (Gorsky et al., 2010), a flatbed scanner generating
129 16-bit gray-level high-resolution images (2400 dpi, pixel size: 10.56 μ m, image size: 15 \times 24 cm equivalent to
130 14 200 \times 22 700 pixels). It is well suited for the imaging of preserved organisms ranging in size from 300 μ m to
131 several centimeters. The ZooScan is run by the custom made, ImageJ based, ZooProcess software which generates
132 one single large image for each scan that contains up to 2000 organisms depending on the size of the imaged
133 organisms.

134 Prior to digitization, the seawater and formaldehyde solution was filtered through a 180 μ m mesh sieve
135 into a trash tank, under a fume hood. The organisms were then gently but thoroughly rinsed with freshwater over
136 the tank, in the sieve. They were then size-fractionated with a 1 mm sieve, into organisms larger and smaller than
137 1 mm size fractions. This size splitting step is recommended when using the ZooScan to address the possible
138 under-representation of large objects bias caused by the necessary subsampling. Each size fraction was subsampled
139 separately with a Motoda splitter to obtain two subsamples containing 500-1000 objects for the large organisms
140 size fraction, and 1000-2000 objects for the small organisms size fraction. Each subsample was imaged after
141 manual separation of objects on the scanning tray, to mitigate the number of overlapping objects as recommended
142 in Vandromme et al. (2012). Overall, 699 samples were digitized following this protocol, corresponding to 1397
143 scans (one sample was not size fractionated as it did not contained organisms larger than 1 mm).

144



145

146 Figure 1: Metazoan zooplankton sampling locations during the PELGAS cruises in the Bay of Biscay from 2004
 147 to 2019. The years with the poorest coverage are 2005 and 2006 with 41 and 43 sampling stations respectively;
 148 and the years with the best coverage are 2015, 2017 and 2019 with 64, 64 and 65 sampling stations respectively.

149 **2.2.2 Digitization with the ZooCAM**

150 The ZooCAM is an in-flow imaging instrument, designed to digitize preserved as well as live zooplankton
151 samples, on board, immediately after net collection (Colas et al., 2018). The ZooCAM features a cylindrical
152 transparent tank in which the zooplankton sample is mixed with filtered seawater. Depending on the richness of
153 the sample, and the subsampling (if necessary), the volume of seawater can be adjusted between 2-7 litres. The
154 organisms were pumped at a $1\text{L}\cdot\text{min}^{-1}$ from the tank to a flowcell inserted between a CCD camera (pixel size: 10.3
155 μm) and a red LED flashing device where they were imaged at 16 fps. Given the flowcell volume, the size of the
156 field of view, the imaging frequency and the flowrate, all the seawater volume containing the organisms was
157 imaged (Colas et al., 2018). Before all the initial volume was imaged, the tank and the tubing were carefully and
158 thoroughly rinsed with filtered seawater to ensure the imaging of all the organisms poured in the tank. For each
159 sample, the ZooCAM generates a stack of small size ($\sim 1\text{ Mo}$) raw images that are subsequently analysed with the
160 ZooCAM software. Depending on the initial water content of the tank and the rinsing, a ZooCAM run can generate
161 up to 10k raw images from which the individual organism vignettes will be extracted. A ZooCAM run on a live
162 sample often generates up to 5000-10000 vignettes of individual organisms. It is very important to subsample the
163 initial samples with a dichotomic splitter (here a Motoda splitter), to get subsamples with a quantity of objects that
164 reduce the risk of imaging overlapping objects, and avoid any dependency to the water volume imaged to
165 reconstruct quantitative estimates of zooplankton as the initial and rinsing volume are variable. Overall, 190
166 samples were digitized live on-board with the ZooCAM.

167 **2.3 Images processing**

168 Both instruments generate grey level working images (8 bit encoding, 0 = black, 255 = white). In both
169 cases, image processing consisted in (i) a “physical” background homogenization by subtracting an empty
170 background image to each sample image (1 for ZooScan, and as many as raw images for ZooCAM), (ii) a
171 thresholding of each raw image (threshold value: 243 for ZooScan, 240 for ZooCAM), (iii) the segmentation of
172 each object imaged. The ZooProcess software was set to detect and segment objects with an area equal or larger
173 than 631 pixels, whereas the ZooCAM software was set to detect objects with an area equal or larger than 667
174 pixels, which in both cases equals $300\ \mu\text{m}$ ESD, or a biovolume of $0.014\ \text{mm}^3$ (using a spherical biovolume model,
175 Vandromme et al., 2012).

176 Morphological features were then extracted on each detected object. Features generated by the ZooScan
177 are defined in Gorsky et al. (2010) and those generated by the ZooCAM are defined in Colas et al. (2018). ZooScan
178 images were processed with ZooProcess v7.39 (04/10/2020) open source software. ZooCAM images were
179 processed with the proprietary ZooCAM custom made software which uses the MIL (Matrox Imaging Library,
180 Dorval, Québec, Canada) as the individual object processing kernel. Each detected object was finally cropped from
181 the working sample images, and saved as a unique, labelled vignette, in a sample specific folder along with a
182 sample specific single text file containing the objects features arranged as a table with objects arranged in lines
183 and features in columns.

184 **2.4 Touching objects**

185 The ZooProcess features a tool that enable the digital separation of possible touching objects in the final
186 image dataset, for each sample. As touching objects may impair the estimations of abundances and size structure

187 (Vandromme et al., 2012), remaining touching objects were searched for on the individual vignettes from the
188 ZooScan and digitally manually separated with the ZooProcess separation tool to improve the quality of further
189 identifications, counts and size structure of zooplankton. The ZooCAM software does not offer such a tool.

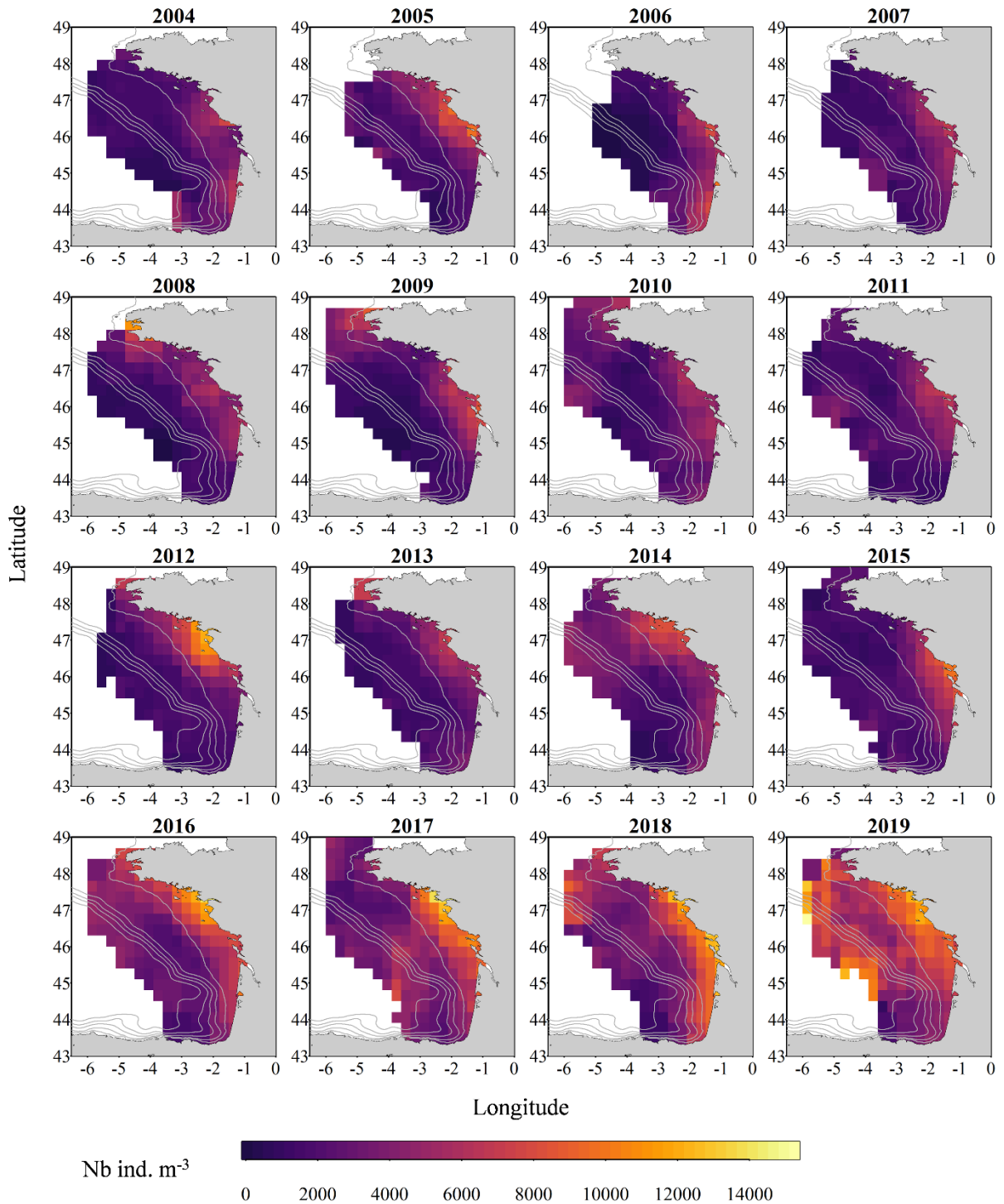
190 **2.5 Taxonomic identification of individual images**

191 All individual vignettes from both instruments were sorted and identified with the help of the online
192 application Ecotaxa (Picheral et al., 2017), as two instrument-specific separated sets. Ecotaxa features a Random
193 Forest algorithm (Breiman, 2001) and a series of instruments specific tuned spatially sparse Convolutional Neural
194 Networks (Graham, 2014) that were used in a combined approach to predict identifications of unidentified objects.
195 First, an automatic classification of non-identified individual vignettes into coarse zooplankton and non-
196 zooplankton categories was carried out. In both cases (ZooScan and ZooCAM), Ecotaxa hosted instrument specific
197 image datasets, previously curated and freely available, that were used as initial learning sets. These initial
198 classifications were then visually inspected, manually validated or corrected when necessary, and taxonomically
199 refined when possible. After a few thousand images were validated in each project, they were used as dataset
200 specific learning sets to improve the initial coarse automatic identifications. This process was iterated until all the
201 individual vignettes were classified into their maximum reachable taxonomical detail. A subsequent quality check
202 of automatic taxonomic identifications has been realized in a two-step process: a first complete review (validation
203 and / or correction) of all individual automatic identifications was done by GN and RJB; then, trained experts (JL
204 and NA) reviewed and curated the ZooScan and the ZooCAM datasets, respectively, at the individual level.
205 Although some identification errors may still remain in the datasets, we consider this double check process as
206 sufficient to provide taxonomically qualified data.

207 **2.6 Intercalibration of the two instruments**

208 The two datasets are usable separately. However, considered together they build a 16 years long spatio-
209 temporal time series. A comparison study was done to ensure these datasets are homogeneous and can thus be
210 combined for ecological studies (Grandremy et al., 2023b). All the zooplankton samples from year 2016 (61
211 sampling stations over the whole BoB continental shelf) were imaged with both instruments. In brief, all non-
212 zooplankton and touching objects images were removed from the initial datasets. Then, the interoperable size
213 range was determined with an assessment based on the comparison of Normalized Biovolume – Size Spectra (NB-
214 SS) for each instrument. This size interval ranges between [0.3-3.39] mm ESD. Finally, the zooplankton
215 communities as seen by the ZooScan and the ZooCAM were compared by taxa and by station using 27 taxonomic
216 groups. Poorly represented taxa as well as non-taxonomically identified objects were not taken into account in the
217 zooplankton variables computation and in community structure analyses. Both instruments showed similar NB-
218 SS slopes for 58 out of 61 stations; depicted equivalent abundances, biovolumes and mean organisms' sizes, as
219 well as similar community composition for a majority of sampling stations. They also estimated similar spatial
220 patterns of the zooplankton community at the scale of the Bay of Biscay. However, some taxonomic groups showed
221 discrepancies between instruments, which originates from the differences in sample preparation protocols before
222 the image acquisition, the imaging techniques and quality, and whether the samples were imaged live or fixed. For
223 example, the mineralized protists (here, Rhizaria) dissolve in formalin and are considered underestimated in
224 preserved seawater samples (Biard et al., 2016). Also, the random orientation of objects in the ZooCAM flow cell
225 leads to a loss of taxonomic identification accuracy due to the difficulty to spot the specific features needed for the

226 identification (Colas et al., 2018; Grandremy et al., 2023b). This is particularly acute for copepods, where the
227 ZooScan seems to provide better identification capabilities to experts, as the organisms are imaged in a lateral
228 view most of the time whereas the ZooCAM often images them in a non-lateral, randomly-oriented view,
229 preventing the visualisation of specific features. A detailed discussion about how to explain the discrepancies
230 between the ZooScan and the ZooCAM can be found in Grandremy et al. (2023b). We assume that the two
231 presented datasets build a single, 16 years long spatio-temporal time series of abundances (Fig. 2) and sizes of
232 zooplanktonic organisms (Fig. 3), from which biovolumes, biomasses, Shannon index (Fig. 4), and zooplankton
233 community size structure can be derived (Vandromme et al., 2012).



234

235 Figure 2: Gridded maps of total zooplankton abundances expressed as individuals per cubic meters of sampled
 236 seawater, during the PELGAS cruises in the Bay of Biscay from 2004 to 2019. The abundances are well within
 237 the range of zooplankton abundances seen over other temperate continental shelves. They exhibit a marked coastal
 238 to offshore gradient, abundances being higher at the coast. Abundances also show an overall increase over the
 239 years. The gridding procedure is presented in Petitgas et al. (2009) and Petitgas et al. (2014). See also Doray et al.
 240 (2018c) and Grandremy et al. (2023a) for application examples.

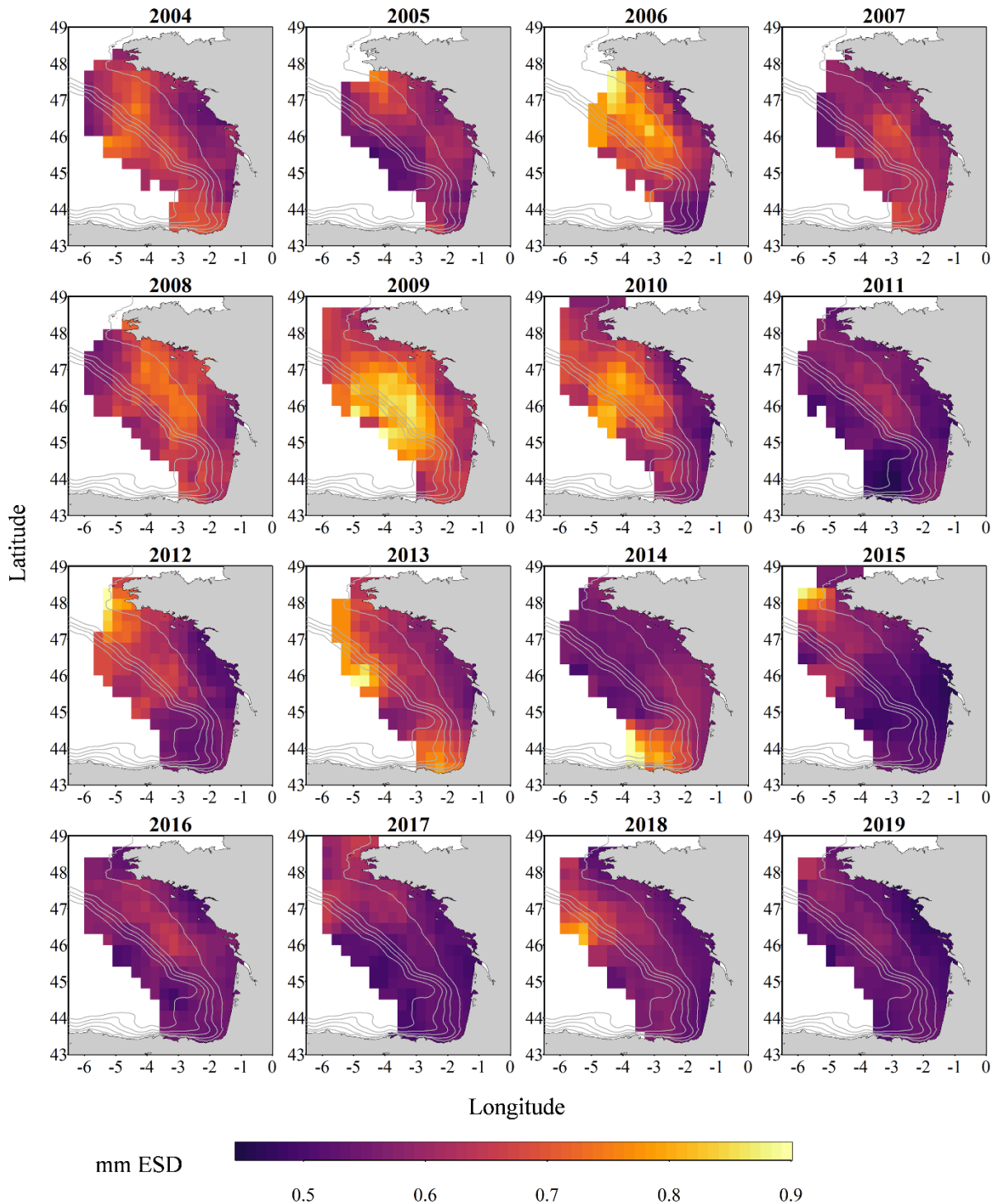


Figure 3: Gridded maps of total zooplankton mean sizes expressed as mm Equivalent Spherical Diameter during the PELGAS cruise in the Bay of Biscay from 2004 to 2019. They exhibit a coastal to offshore gradient as well as a north-south gradient. Mean body sizes are smaller at the coast and usually smaller in the south. In general, mean body sizes show an overall decrease over the years. The gridding procedure is presented in Petitgas et al. (2009) and Petitgas et al. (2014). See also Doray et al. (2018c) and Grandremy et al. (2023a) for application examples.

247 **3 Datasets**

248 **3.1 Taxonomic groups and Operational Morphological Groups**

249 The ZooScan dataset is composed of 1,153,507 zooplankton individuals, zooplankton parts, non-living
250 particles and imaging artefacts individually imaged and measured with the ZooScan and ZooProcess (Gorsky et
251 al., 2010), sorted in 127 taxonomic and morphological groups. The ZooCAM dataset is composed of 702,111
252 zooplankton individuals, zooplankton parts, non-living particles and imaging artefacts individually imaged and
253 measured with the ZooCAM (Colas et al., 2018), sorted in 127 taxonomic and morphological or life stages groups.
254 The total number of different groups identified with both instruments combined is 170, among which 84 are in
255 common (Table 1), 43 belong to the ZooScan dataset only and 43 others belong to the ZooCAM dataset only
256 (Table 2). The identified groups were divided into actual taxa and Operational Morphological Groups (OMGs).
257 Typically, OMGs are either non-adult life stages of taxa, aggregated morphological groups, or non-living groups
258 (see Tables 1 and 2). Among the groups common to both instruments, 45 are actual taxa, and 39 are OMGs (Table
259 1). Among the ZooScan only groups, 22 are taxa, and 21 are OMGs, and among the ZooCAM only groups, 18 are
260 taxa, and 25 are OMGs (Table 2).

261 The differences in identified groups, in the ratio taxa/OMGs, and in the associated counts arose from
262 several aspects of the data generation. Firstly, the two imaging methods differ in their technical set-up. The main
263 difference is that, on the one hand, fixed organisms are laid down and arranged manually on the imaging sensor
264 and digitized in a lab, steady 2-D, set-up when using the ZooScan. On the other hand, organisms are imaged live,
265 in a moving fluid, in a 3-D environment (the flowcell), on-board when digitized with the ZooCAM. Their position
266 in front of the camera may not enable an identification as precise as when they are laid on the scanner tray
267 (Grandremy et al., 2023b; Colas et al., 2018). Secondly, the dataset are sequential in time, the ZooCAM dataset
268 follows the ZooScan's. Zooplankton communities in the Bay of Biscay may have changed over time, even if their
269 biomass as aggregated groups show a remarkable space-time stability (Grandremy et al., 2023a). Thirdly, we
270 cannot guaranty that there is no adverse effect on taxonomic identification, as validation involved several experts
271 (Culverhouse, 2007). Although we paid great attention to homogenize the final detailed datasets, we recommend
272 to aggregate taxa and OMGs and reduce the biological resolution for ecological studies (Grandremy et al., 2023a,
273 2023b). Additionally, numerous identified and sorted taxa and OMGs do not belong to the metazoan zooplankton,
274 or are non-adult life stages, or parts of organisms. Those were included in the presented datasets because they are
275 always found in natural samples. They need to be separated from entire organisms to ensure as accurate as possible
276 abundances estimations, as well as taken into account to ensure accurate biovolumes or biomasses estimations. A
277 good example is the siphonophore issue: numerous swimming bells of degraded siphonophores individuals can be
278 found and imaged in a sample. Determining an accurate siphonophore abundance may not be easy, but this could
279 be overcome by considering the biovolume or biomass of siphonophores by adding up the numerous parts'
280 biovolumes or biomass of the organisms imaged.

281 Table 1: ZooCAM and ZooScan common taxa and Operational Morphological Groups (OMGs). Taxa are listed
282 in the left column of the table, and OMGs are listed in the right column of the table . OMGs names are spelled as
283 they appear in the dataset. Numbers next to each taxa and OMGs are the counts and the percentages (%) for each
284 category for each instrument in the whole datasets. Non-zooplanktonic OMGs are highlighted in bold, and genera
285 and species are formatted in italics.

| taxa | ZooCAM | | ZooScan | | OMG | ZooCAM | | ZooScan | |
|----------------------|--------|--------|---------|--------|---------------------------------------|--------|--------|---------|--------|
| | counts | % | counts | % | | counts | % | counts | % |
| Calanoida | 137536 | 19.58 | 149956 | 13.00 | detritus | 105751 | 15.06 | 219541 | 19.03 |
| Oithonidae | 112977 | 16.09 | 110510 | 9.58 | diatoma | 36842 | 5.25 | 1084 | 0.09 |
| Acartiidae | 30403 | 4.33 | 66353 | 5.75 | bubble | 32563 | 4.64 | 1112 | 0.10 |
| Temoridae | 13520 | 1.93 | 31335 | 2.72 | Noctiluca_Noctilucaeae | 22165 | 3.16 | 20784 | 1.80 |
| Oncaeidae | 11843 | 1.69 | 34651 | 3.00 | other_living | 15029 | 2.14 | 5861 | 0.51 |
| Calanidae | 9578 | 1.36 | 91513 | 7.93 | dead_copepoda | 13383 | 1.91 | 17151 | 1.49 |
| Limacinidae | 8966 | 1.28 | 6423 | 0.56 | fiber_detritus | 13379 | 1.91 | 25124 | 2.18 |
| Appendicularia | 6724 | 0.96 | 34027 | 2.95 | nauplii_cirripedia | 6766 | 0.96 | 6008 | 0.52 |
| Cladocera | 5590 | 0.80 | 18213 | 1.58 | gonophore_diphyidae | 4395 | 0.63 | 1462 | 0.13 |
| Centropagidae | 4592 | 0.65 | 14651 | 1.27 | multiple_copepoda | 3740 | 0.53 | 961 | 0.08 |
| <i>Neoceratium</i> | 2984 | 0.43 | 4830 | 0.42 | nauplii_crustacea | 3422 | 0.49 | 10747 | 0.93 |
| Euchaetidae | 2643 | 0.38 | 12957 | 1.12 | artefact | 2643 | 0.38 | 60718 | 5.26 |
| Metridinidae | 2333 | 0.33 | 15081 | 1.31 | multiple_other | 1928 | 0.27 | 10303 | 0.89 |
| Corycaeidae | 2021 | 0.29 | 4720 | 0.41 | pluteus_echinodermata | 1623 | 0.23 | 1441 | 0.12 |
| <i>Euterpina</i> | 1043 | 0.15 | 2870 | 0.25 | calyptopsis_euphausiacea | 1396 | 0.20 | 3246 | 0.28 |
| Euphausiacea | 889 | 0.13 | 1195 | 0.10 | bivalvia_mollusca | 1324 | 0.19 | 3766 | 0.33 |
| <i>Calocalanus</i> | 820 | 0.12 | 1196 | 0.10 | bract_diphyidae | 1315 | 0.19 | 386 | 0.03 |
| Chaetognatha | 624 | 0.09 | 7274 | 0.63 | cypris | 862 | 0.12 | 2363 | 0.20 |
| Harpacticoida | 481 | 0.07 | 1697 | 0.15 | nectophore_diphyidae | 839 | 0.12 | 14389 | 1.25 |
| <i>Obelia</i> | 459 | 0.07 | 1016 | 0.09 | egg_actinopterygii | 768 | 0.11 | 3596 | 0.31 |
| Annelida | 256 | 0.04 | 2434 | 0.21 | tail_appendicularia | 753 | 0.11 | 11349 | 0.98 |
| Decapoda | 173 | 0.02 | 471 | 0.04 | cyphonaute | 684 | 0.10 | 2218 | 0.19 |
| <i>Microsetella</i> | 116 | 0.02 | 1169 | 0.10 | eudoxie_diphyidae | 501 | 0.07 | 69 | 0.01 |
| Phoronida | 90 | 0.01 | 163 | 0.01 | larvae_echinodermata | 483 | 0.07 | 2200 | 0.19 |
| Actinopterygii | 85 | 0.01 | 2113 | 0.18 | part_siphonophorae | 279 | 0.04 | 12976 | 1.12 |
| Candaciidae | 70 | 0.01 | 2773 | 0.24 | larvaeannelida | 244 | 0.03 | 708 | 0.06 |
| Amphipoda | 68 | 0.01 | 853 | 0.07 | egg_sac_egg | 152 | 0.02 | 394 | 0.03 |
| Tomopteridae | 58 | 0.01 | 618 | 0.05 | zoa_decapoda | 151 | 0.02 | 1405 | 0.12 |
| Ostracoda | 55 | 0.01 | 341 | 0.03 | cnidaria_metazoa | 148 | 0.02 | 4974 | 0.43 |
| Doliolida | 26 | < 0.01 | 128 | 0.01 | larvae_porcellanidae | 127 | 0.02 | 2838 | 0.25 |
| Echinodermata | 24 | < 0.01 | 253 | 0.02 | nectophore_physonectae | 106 | 0.02 | 696 | 0.06 |
| Aetideidae | 15 | < 0.01 | 75 | 0.01 | ctenophora_metazoa | 94 | 0.01 | 126 | 0.01 |
| <i>Branchiostoma</i> | 15 | < 0.01 | 210 | 0.02 | egg_unkn temp_Engraulidae temp | 61 | 0.01 | 192 | 0.02 |
| Thecosomata | 15 | < 0.01 | 59 | 0.01 | part_ctenophora | 30 | < 0.01 | 319 | 0.03 |
| Heterorhabdidae | 8 | < 0.01 | 205 | 0.02 | tornaria larvae | 21 | < 0.01 | 83 | 0.01 |
| Pontellidae | 6 | < 0.01 | 299 | 0.03 | egg_other | 17 | < 0.01 | 2281 | 0.20 |
| Cumacea | 4 | < 0.01 | 180 | 0.02 | megalopa | 6 | < 0.01 | 460 | 0.04 |
| Mysida | 3 | < 0.01 | 885 | 0.08 | scale | 2 | < 0.01 | 53 | < 0.01 |
| Eucalanidae | 2 | < 0.01 | 839 | 0.07 | siphonula | 1 | < 0.01 | 20 | < 0.01 |
| Insecta | 2 | < 0.01 | 3 | < 0.01 | | | | | |
| Foraminifera | 1 | < 0.01 | 384 | 0.03 | | | | | |
| <i>Haloptilus</i> | 1 | < 0.01 | 5 | < 0.01 | | | | | |
| Isopoda | 1 | < 0.01 | 123 | 0.01 | | | | | |
| Rhincalanidae | 1 | < 0.01 | 127 | 0.01 | | | | | |
| Sapphirinidae | 1 | < 0.01 | 21 | < 0.01 | | | | | |

287 Table 2: ZooCAM and ZooScan not common taxa and Operational Morphological Groups (OMGs). Taxa and
288 OMGs appearing exclusively in the ZooCAM dataset are listed in the left column, those appearing exclusively in
289 the ZooScan dataset are listed in the right column. OMGs names are spelled as they appear in the dataset. Numbers
290 next to each taxa and OMG are the counts and the percentages (%) for each category for each instrument in the
291 whole datasets. Non-zooplanktonic taxa and OMGs are highlighted in bold, and genera and species are formatted
292 in italics.

| ZooCAM | | | ZooScan | | |
|--------------------------------|--------|--------|----------------------------------|--------|--------|
| taxa/OMG | counts | % | taxa/OMG | counts | % |
| light_detritus | 38126 | 5.43 | badfocus_artefact | 34507 | 2.99 |
| Rhizaria | 13347 | 1.90 | badfocus_Copepoda | 11656 | 1.01 |
| Copepoda X | 6727 | 0.96 | Eumalacostraca | 9815 | 0.85 |
| fluffy_detritus | 3589 | 0.51 | part_Crustacea | 7530 | 0.65 |
| <i>Evadne</i> | 1889 | 0.27 | Fritillariidae | 3635 | 0.32 |
| Hydrozoa | 1674 | 0.24 | trunk_appendicularia | 1210 | 0.10 |
| Poecilostomatoida | 1094 | 0.16 | <i>Aglaura</i> | 1113 | 0.10 |
| Rhizaria X | 857 | 0.12 | <i>Pleuromamma</i> | 695 | 0.06 |
| Rhizosolenids | 761 | 0.11 | part_Cnidaria | 692 | 0.06 |
| dead_harpacticoida | 528 | 0.08 | zoaea_galatheidae | 660 | 0.06 |
| gelatinous | 348 | 0.05 | pluteus_ophiuroida | 640 | 0.06 |
| <i>Trichodesmium</i> | 265 | 0.04 | Salpida | 470 | 0.04 |
| aggregata | 253 | 0.04 | Harosa | 374 | 0.03 |
| feces | 227 | 0.03 | tail_chaetognatha | 251 | 0.02 |
| <i>Halosphaera</i> | 193 | 0.03 | <i>Euchirella</i> | 239 | 0.02 |
| <i>Podon</i> | 162 | 0.02 | protozoa_mysida | 229 | 0.02 |
| Diphyidae | 144 | 0.02 | <i>Solmundella bitentaculata</i> | 178 | 0.02 |
| larvae_gastropoda | 116 | 0.02 | Peltidiidae | 133 | 0.01 |
| chainlarge | 114 | 0.02 | <i>Liriope tetraphylla</i> | 121 | 0.01 |
| veliger | 113 | 0.02 | part_Annelida | 121 | 0.01 |
| egg 1 temp_Sardina temp | 100 | 0.01 | larvae_crustacea | 114 | 0.01 |
| egg 1 temp_Engraulidae temp | 65 | 0.01 | larvae_mysida | 73 | 0.01 |
| Isias | 51 | 0.01 | ephyra_scyphozoa | 64 | 0.01 |
| egg 2 3 temp_Sardina temp | 49 | 0.01 | actinula_hydrozoa | 49 | < 0.01 |
| Calycophorae | 30 | < 0.01 | part_thaliacea | 44 | < 0.01 |
| egg 9 11 temp_Sardina temp | 26 | < 0.01 | <i>Atlanta</i> | 43 | < 0.01 |
| egg unkn temp_Sardina temp | 23 | < 0.01 | like_laomediidae | 36 | < 0.01 |
| <i>Calocalanus tenuis</i> | 17 | < 0.01 | Nemertea | 31 | < 0.01 |
| egg 4 6 temp_Sardina temp | 15 | < 0.01 | protozoa_penaecidae | 28 | < 0.01 |
| egg 9 11 temp_Engraulidae temp | 14 | < 0.01 | Cavoliniidae | 21 | < 0.01 |
| egg 7 8 temp_Engraulidae temp | 13 | < 0.01 | Actiniaria | 13 | < 0.01 |
| Enteropneusta_Hemichordata | 12 | < 0.01 | pilidium_nemertea | 12 | < 0.01 |
| <i>Chaetoceros sp.</i> | 9 | < 0.01 | protozoa_sergestidae | 12 | < 0.01 |
| head_crustacea | 9 | < 0.01 | phyllosoma | 8 | < 0.01 |
| <i>Centropages hamatus</i> | 8 | < 0.01 | Creseidae | 7 | < 0.01 |
| Thaliacea | 7 | < 0.01 | Penaecioidea | 7 | < 0.01 |
| egg 4 6 temp_Engraulidae temp | 6 | < 0.01 | Paguridae | 4 | < 0.01 |
| Sphaeronectidae | 4 | < 0.01 | larvae_squillidae | 4 | < 0.01 |
| <i>Thalassionema</i> | 4 | < 0.01 | Cephalopoda | 3 | < 0.01 |
| egg 2 3 temp_Engraulidae temp | 3 | < 0.01 | <i>Cymbulia peroni</i> | 3 | < 0.01 |
| <i>Jaxea</i> | 2 | < 0.01 | Nannosquillidae | 2 | < 0.01 |
| <i>Pyrosoma</i> | 1 | < 0.01 | <i>Lubbockia</i> | 1 | < 0.01 |
| larvae_ascidiacea | 1 | < 0.01 | Monstrilloida | 1 | < 0.01 |

293

294

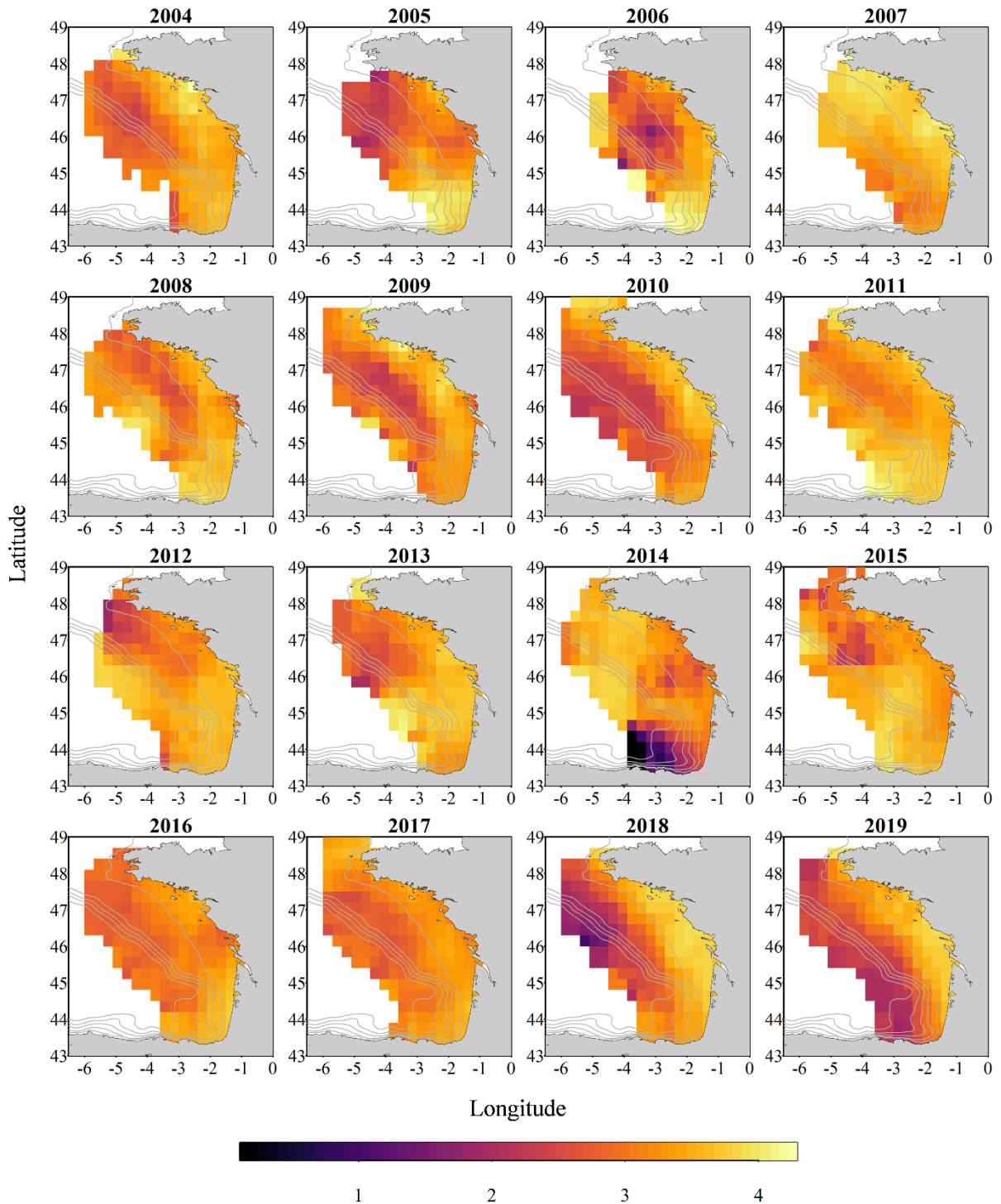
295 OMGs' names are mainly in the form of two words separated by a "<" character. Although we tried to name them
 296 as most explicitly as possible, a few potentially needed clarifications can be found in Table 3.

297 Table 3: Non-exhaustive list of prefixes, their types (morphological, developmental stage, taxonomical, non-living
 298 and imaging artefact), and content.

| prefix | type | content of category |
|---------------|---------------------|---|
| bract | morphological | single siphonophorae bracts |
| eudoxie | morphological | single siphonophorae eudoxia zooids |
| gonophore | morphological | single siphonophorae gonozooids |
| nectophore | morphological | single siphonophorae swimming bells |
| trunk | morphological | single appendicularian trunks detached from their tails |
| tail | morphological | appendicularian's or chaetognath's tail shaped part of the body |
| head | morphological | individual organisms' heads detached from the body |
| part | morphological | unidentified body part |
| egg sac | morphological | detached copepod egg sacs |
| like | morphological | look alike, without absolute certainty |
| multiple | morphological | two or more objects touching each other in the same vignette |
| other | morphological | non-identified living object |
| actinula | developmental stage | undefined hydrozoa actinula larval stage |
| calyptopsis | developmental stage | Euphausiacea calyptopsis larval stage |
| egg | developmental stage | egg larval stage |
| ephyra | developmental stage | ephyra hydrozoa larval stage |
| larvae | developmental stage | undefined larval stage |
| nauplii | developmental stage | crustacean nauplii larval stage |
| pilidium | developmental stage | free-swimming larvae of nemertean worm |
| protozoa | developmental stage | crustacean protozoa larval stage |
| pluteus | developmental stage | Echinodermata pluteus larval stage |
| zoea | developmental stage | crustacean zoea larval stage |
| egg 1 temp | developmental stage | clupeid fish embryo developmental stage 1* |
| egg 2 3 temp | developmental stage | clupeid fish embryo developmental stages 2 and 3 aggregated* |
| egg 4 6 temp | developmental stage | clupeid fish embryo developmental stages 4 to 6 aggregated* |
| egg 7 8 temp | developmental stage | clupeid fish embryo developmental stages 7 and 8 aggregated* |
| egg 9 11 temp | developmental stage | clupeid fish embryo developmental stages 9 to 11 aggregated* |
| egg unknown | developmental stage | clupeid fish unidentified embryo developmental stage* |
| Bivalvia | taxonomical | small bivalve larvae of unidentified mollusca |
| dead | non-living | copepod's exuvia, carcass or part of dead body |
| fiber | non-living | fiber like detritus |
| fluffy | non-living | very porous detritic particles |
| light | non-living | very transparent detritic particles |
| badfocus | imaging artefact | out-of-focus objects |

299

300 * clupeids fish embryo developmental stages according to Ahlstrom (1943) and Moser & Ahlstrom (1985).



301

302 Figure 4: Gridded maps of total zooplankton Shannon index (calculated on spherical biovolumes) during the
 303 PELGAS cruise in the Bay of Biscay from 2004 to 2019. Shannon index exhibit a coastal to offshore gradient as
 304 well as a north-south gradient. Shannon index is larger at the coast and in the south, except in 2014 where it is
 305 smaller in the south, offshore. The gridding procedure is presented in Petitgas et al. (2009) and Petitgas et al.
 306 (2014). See also Doray et al. (2018c) and Grandremy et al. (2023a) for application examples.

307 3.2 Data and images

308 3.2.1 Data

309 The data is divided into two datasets available as tab separated files, one for each instrument. Within each
310 dataset the data is organized as a table containing text data as well as numerical data. Each dataset combines
311 together actual data and metadata at the individual object granularity. For each object, the user will be able to find
312 descriptors originating from the image processing (i.e. features), and sampling metadata (i.e. latitude and longitude
313 of sampling station, date and time of sampling, sampling device, etc.) and sample processing metadata (i.e.
314 subsampling factor, seawater sampled volume, pixel size), in columns, and individual objects in lines. The columns
315 headers are defined in Tables A1 and A2 for ZooCAM and ZooScan datasets respectively. The following prefixes
316 enable the segregation of types of data and metadata: (i) “object_”, which identifies variables assigned to each
317 object individually; (ii) “sample_”, which identifies variables assigned to each sample; (iii) “acq_”, which
318 identifies variables assigned to each data acquisition for the same sample (note here that this type of variable is
319 found only in the ZooScan dataset as ZooScan samples were splitted in two size fractions corresponding to two
320 acquisitions); (iv) “process_”, which identifies variables describing key image processing features (i.e. pixel size).
321 Those prefixes originate from the use of the Ecotaxa web application to sort and identify the images (Picheral et
322 al., 2017) that promote this specific formatting. The ZooCAM dataset is shaped as a 72 columns (variables) x
323 702,111 rows (individual imaged objects) matrix and the ZooScan dataset is shaped as a 71 columns (variables) x
324 1,153,507 rows (individual imaged objects) matrix.

325 Among the 70+ variables it is worth noticing the following ones:

- 326 (i) objid: it is a unique individual object numerical identifier that enables to link single data line to a
327 corresponding single image in the image dataset;
- 328 (ii) taxon: it is the taxonomic or OMG identification of the imaged objects written as they appear in the
329 Tables 1 and 2;
- 330 (iii) lineage: it is the full taxonomic lineage of the taxon. Lineage may be used to aggregate taxa at a higher
331 taxonomic levels, respecting taxonomic lineages;
- 332 (iv) classif_id: it is a unique, numerical, taxon identifier;
- 333 (v) sample_sub_part / acq_sub_part: those are the subsampling ratios, for ZooCAM and ZooScan
334 respectively, needed to reconstruct the quantitative estimates of the samples’ abundances;
- 335 (vi) sample_fishingvolume / sample_tot_vol: those are the total seawater sampled volumes for ZooCAM
336 and ZooScan respectively, needed to normalize the samples’ concentrations by seawater volume.

337 One can therefore calculate quantitative abundances estimates for a taxon in a sample as follow:

$$338 \text{ ZooCAM: } Ab_{\text{taxon}} = \frac{n_{\text{taxon}} \times \text{sample_sub_part}}{\text{sample_fishingvolume}} \quad (1)$$

$$339 \text{ ZooScan: } Ab_{\text{taxon}} = \frac{(n_{\text{taxon}_{\text{acq1}}} \times \text{acq_sub_part}_{\text{acq1}}) + (n_{\text{taxon}_{\text{acq2}}} \times \text{acq_sub_part}_{\text{acq2}})}{\text{sample_tot_vol}} \quad (2)$$

340 Where Ab is the abundance in ind.m^{-3} and n is the number of individuals for “taxon”.

341 **3.2.2 Images**

342 Two sets of individual images sorted into folders by categories (Tables 1 and 2) come along with each
343 dataset. For the ZooCAM only, the associated images from years 2016 and 2017 contain printed Region Of Interest
344 (ROI) bounding box limits and text at the bottom of each image, and non-homogenised background within and
345 around the ROI bounding box; images from year 2018 contain non-homogenised background within the ROI
346 bounding box only; images from 2019 have a completely homogeneous and thresholded background around the
347 object. The differences arose from successive ZooCAM software updates that do not modify the calculation of
348 object's features. The ZooScan images have all a completely homogeneous and thresholded background around
349 the object, no bounding box limits nor text printed in the images. All images for the two instruments datasets have
350 a 1 mm scale bar printed at the bottom left corner.

351 **4 Data availability**

352 The ZooScan dataset can be found as the *PELGAS Bay of Biscay ZooScan zooplankton Dataset (2004-2016)* in
353 the SEANOE dataportal following the link: <https://www.seanoe.org/data/00829/94052/> (doi: 10.17882/94052,
354 Grandremy et al., 2023c). Individual objects images can be freely viewed and explored by anyone using the
355 Ecotaxa (<https://ecotaxa.obs-vlfr.fr/>) web application, without registration, under the tab “explore images”, by
356 searching the project name: “*PELGAS Bay of Biscay ZooScan zooplankton Dataset (2004-2016)*”.

357 The ZooCAM dataset can be found as the *PELGAS Bay of Biscay ZooCAM zooplankton Dataset (2016-2019)* in
358 the SEANOE dataportal <https://www.seanoe.org/data/00828/94040/> (doi: 10.17882/94040, Grandremy et al.,
359 2023d). Individual objects images can be freely viewed and explored by anyone using the Ecotaxa
360 (<https://ecotaxa.obs-vlfr.fr/>) web application, without registration, under the tab “explore images”, by searching
361 the project name: “*PELGAS Bay of Biscay ZooCAM zooplankton Dataset (2016-2019)*”.

362 Each dataset comes as a .zip archive that contains:

- 363 • One tab separated file containing all data and metadata associated to each imaged and identified object.
- 364 • One comma separated file containing the name, type, definition and unit of each field (column)
- 365 • One comma separated file containing the taxonomic list of the dataset, with counts and nature of the
366 content of the category
- 367 • A directory “*individual_images*” containing images of each object, named according to the object id
368 *objid* and sorted in subdirectories according to their taxonomic identification, across years and sampling
369 stations.

370 **5 Concluding remarks**

371 Recent studies showed that the small pelagic fish (SPF) communities have suffered from a drastic
372 decrease of condition in the Mediterranean Sea and in the Bay of Biscay (Van Beveren et al., 2014; Doray et al.,
373 2018d; Saraux et al., 2019) over the last 20 years. This loss of condition was especially expressed by the constant
374 decrease of SPF size- and weight-at-age (Doray et al., 2018d; Veron et al. 2020), and possibly explained by a
375 change in SPF trophic resource composition, size and quality (Brosset et al., 2016; Queiros et al., 2019; Menu et
376 al., 2023). Identifying and measuring zooplankton at appropriate temporal and spatial scales is not an easy task,
377 but can be addressed with imaging. These datasets were assembled as an effort to make possible the exploration

378 of the relationship between SPF observed dynamics in the Bay of Biscay and their main food resource's dynamics,
379 the metazoan zooplankton. This zooplankton imaging data series is a significant output of Nina Grandremy PhD
380 (2019-2023), that is currently being exploited (Grandremy et al., 2023a), and is intended to be continued and
381 updated on a yearly basis in the framework of the PELGAS program, to better understand the underlying processes
382 presiding to long-term SPF dynamics. Moreover, those two zooplankton datasets can be associated with the
383 PELGAS survey datasets previously published in 2018, also in the SEANOE dataportal, featuring hydrological,
384 primary producers, fish and megafauna data arranged as gridded data (Doray et al., 2018b). Together, all these
385 datasets allow to study simultaneously all the pelagic ecosystem compartments, with coherent spatial domain (the
386 Bay of Biscay continental shelf), resolution and time series. Nevertheless, a spatial gridding of the data is highly
387 recommended (as represented in the Fig. 2, 3 and 4), since the spatial coverage of the sampling protocols can vary
388 between years (Fig. 1), within and between each pelagic ecosystem compartment. A procedure for such batch data
389 spatial smoothing is presented e.g. in Petitgas et al. (2009) and Petitgas et al. (2014). See also Doray et al. (2018c)
390 and Grandremy et al. (2023a) for application examples. As several descriptors of the spring zooplankton
391 community (abundances, sizes, biovolumes, biomass) can be derived from this 16 years long spatially resolved
392 time series at several taxonomic levels, these datasets are intended to be used in various ecological studies
393 including the zooplankton compartment, especially modelling studies, where zooplankton is usually
394 underrepresented (Mitra, 2010; Mitra et al., 2014). Finally, these datasets can also be used for machine learning
395 applied to plankton studies serving, for example, as consequent learning sets.

396 **Disclaimer**

397 Data are published without any warranty, express or implied. The user assumes all risk arising from his/her use of
398 data. Data are intended to be research-quality, but it is possible that the data themselves contain errors. It is the
399 sole responsibility of the user to assess if the data are appropriate for his/her use, and to interpret the data
400 accordingly. Authors welcome users to ask questions and report problems.

401 **Authors' contributions**

402 GN scanned and validated most of the ZooScan dataset, assembled the datasets, and led the drafting. BP collected
403 and managed the samples since 2004, and participated in the manual validation of identifications. DE scanned a
404 substantial fraction of the ZooScan samples and participated in the initial sorting of vignettes. DMM participated
405 in the collection of samples, and was involved in the ZooCAM development. DM was chief scientist on the
406 PELGAS surveys and participated in the drafting. DC supervised GN work and participated in the drafting. FB
407 developed, improved and maintained the ZooCAM software. JL curated a substantial fraction of the ZooScan
408 dataset manual validation of identifications. HM participated in the collection of samples, lead the DEFIPEL
409 project, and participated in the drafting. LMS participated in the collection of samples, and managed the ZooCAM.
410 NA curated a substantial fraction of the ZooScan and ZooCAM dataset manual validation of identifications. PP
411 supervised GN work and participated in the drafting. PPh participated in the collection of samples and participated
412 in the drafting. RJ supervised the development and improvement of the ZooCAM. TM developed and improved
413 the ZooCAM, and participated in the collection of samples. RJB supervised GN work, participated in the collection
414 of samples, curated a substantial fraction of the ZooCAM dataset manual validation of identifications, and lead
415 the drafting.

416 **Competing interests**

417 The authors declare that they have no conflict of interest.

418 **Acknowledgements**

419 The authors acknowledge receiving funding from the ‘France Filière Pêche’ DEFIPEL project. NG acknowledges
420 the funding of her PhD by Region Pays de la Loire, FR and Ifremer. The authors wish to thank Jean-Yves Coail,
421 Gérard Guyader and Patrick Berriet (Ifremer – REM-RDT-SIIM) for their contribution to the hardware assembly
422 of the ZooCAM. The authors acknowledge the work of Elio Raphalen for scanning year 2005 samples. The authors
423 thank the EMBRC platform PIQs for image analysis. This work was supported by EMBRC-France, whose French
424 state funds are managed by the ANR within the Investments of the Future program under reference ANR-10-
425 INBS-02. Finally, the authors wish also to thank the many other students, technicians and scientists who
426 participated in the sampling and samples imaging on board, and the successive crews of the R/V *Thalassa* involved
427 in the PELGAS surveys from 2004 to 2019.

428

429 **References**

- 430 Ahlstrom, E.H., 1943. Studies on the Pacific Pilchard Or Sardine (*Sardinops Caerulea*): Influence of Temperature
431 on the Rate of Development of Pilchard Eggs in Nature. United States Department of the Interior, Fish and Wildlife
432 Service.
- 433 Banse, K., 1995. Zooplankton: Pivotal role in the control of ocean production: I. Biomass and production. ICES
434 Journal of Marine Science 52, 265–277. [https://doi.org/10.1016/1054-3139\(95\)80043-3](https://doi.org/10.1016/1054-3139(95)80043-3)
- 435 Batten, S.D., Abu-Alhaja, R., Chiba, S., Edwards, M., Graham, G., Jyothibabu, R., Kitchener, J.A., Koubbi, P.,
436 McQuatters-Gollop, A., Muxagata, E., Ostle, C., Richardson, A.J., Robinson, K.V., Takahashi, K.T., Verheye,
437 H.M., Wilson, W., 2019. A Global Plankton Diversity Monitoring Program. *Frontiers in Marine Science* 6.
438 <https://doi.org/10.3389/fmars.2019.00321>
- 439 Beaugrand, G., Brander, K.M., Lindley, J.A., Souissi, S., Reid, P.C., 2003. Plankton effect on cod recruitment in
440 the North Sea. *Nature* 426, 661–664. <https://doi.org/10.1038/nature02164>
- 441 Benedetti, F., Jalabert, L., Sourisseau, M., Becker, B., Cailliau, C., Desnos, C., Elineau, A., Irisson, J.-O.,
442 Lombard, F., Picheral, M., Stemmann, L., Pouline, P., 2019. The Seasonal and Inter-Annual Fluctuations of
443 Plankton Abundance and Community Structure in a North Atlantic Marine Protected Area. *Front. Mar. Sci.* 6.
444 <https://doi.org/10.3389/fmars.2019.00214>
- 445 Biard, T., Stemmann, L., Picheral, M., Mayot, N., Vandromme, P., Hauss, H., Gorsky, G., Guidi, L., Kiko, R.,
446 Not, F., 2016. In situ imaging reveals the biomass of giant protists in the global ocean. *Nature* 532, 504–507.
447 <https://doi.org/10.1038/nature17652>
- 448 Breiman, L., 2001. Random forests. *Mach. Learn.* 45, 5–32. <https://doi.org/10.1023/A:1010933404324>

449 Brosset, P., Le Bourg, B., Costalago, D., Banaru, D., Van Beveren, E., Bourdeix, J.-H., Fromentin, J.-M., Menard,
450 F., Saraux, C., 2016. Linking small pelagic dietary shifts with ecosystem changes in the Gulf of Lions. *Mar. Ecol.-*
451 *Prog. Ser.* 554, 157–171. <https://doi.org/10.3354/meps11796>

452 Chiba, S., Batten, S., Martin, C.S., Ivory, S., Miloslavich, P., Weatherdon, L.V., 2018. Zooplankton monitoring to
453 contribute towards addressing global biodiversity conservation challenges. *Journal of Plankton Research* 40, 509–
454 518. <https://doi.org/10.1093/plankt/fby030>

455 Colas, F., Tardivel, M., Perchoc, J., Lunven, M., Forest, B., Guyader, G., Danielou, M.M., Le Mestre, S., Bourriau,
456 P., Antajan, E., Sourisseau, M., Huret, M., Petitgas, P., Romagnan, J.B., 2018. The ZooCAM, a new in-flow
457 imaging system for fast onboard counting, sizing and classification of fish eggs and metazooplankton. *Progress in*
458 *Oceanography, Multidisciplinary integrated surveys* 166, 54–65. <https://doi.org/10.1016/j.pocean.2017.10.014>

459 Culverhouse, P.F., 2007. Human and machine factors in algae monitoring performance. *Ecol. Inform.* 2, 361–366.
460 <https://doi.org/10.1016/j.ecoinf.2007.07.001>

461 Cury, P., Bakun, A., Crawford, R.J.M., Jarre, A., Quiñones, R.A., Shannon, L.J., Verheye, H.M., 2000. Small
462 pelagics in upwelling systems: patterns of interaction and structural changes in “wasp-waist” ecosystems. *ICES*
463 *Journal of Marine Science* 57, 603–618. <https://doi.org/10.1006/jmsc.2000.0712>

464 Doray, M., Boyra, G., van der Kooij, J., 2021. ICES Survey Protocols - Manual for acoustic surveys coordinated
465 under ICES Working Group on Acoustic and Egg Surveys for Small Pelagic Fish (WGACEGG).
466 <https://doi.org/10.17895/ICES.PUB.7462>

467 Doray, M., Petitgas, P., Romagnan, J.B., Huret, M., Duhamel, E., Dupuy, C., Spitz, J., Authier, M., Sanchez, F.,
468 Berger, L., Dorémus, G., Bourriau, P., Grellier, P., Massé, J., 2018a. The PELGAS survey: Ship-based integrated
469 monitoring of the Bay of Biscay pelagic ecosystem. *Progress in Oceanography, Multidisciplinary integrated*
470 *surveys* 166, 15–29. <https://doi.org/10.1016/j.pocean.2017.09.015>

471 Doray, M., Huret, M., Authier, M., Duhamel, E., Romagnan, J.-B., Dupuy, C., Spitz, J., Sanchez, F., Berger, L.,
472 Dorémus, G., Bourriau, P., Grellier, P., Pennors, L., Masse, J., Petitgas, P., 2018b. Gridded maps of pelagic
473 ecosystem parameters collected in the Bay of Biscay during the PELGAS integrated survey.
474 <https://doi.org/10.17882/53389>

475 Doray, M., Hervy, C., Huret, M., Petitgas, P., 2018c. Spring habitats of small pelagic fish communities in the Bay
476 of Biscay. *Progress in Oceanography, Multidisciplinary integrated surveys* 166, 88–108.
477 <https://doi.org/10.1016/j.pocean.2017.11.003>

478 Doray, M., Petitgas, P., Huret, M., Duhamel, E., Romagnan, J.B., Authier, M., Dupuy, C., Spitz, J., 2018d.
479 Monitoring small pelagic fish in the Bay of Biscay ecosystem, using indicators from an integrated survey. *Progress*
480 *in Oceanography* 166, 168–188. <https://doi.org/10.1016/j.pocean.2017.12.004>

481 Elineau, A., Desnos, C., Jalabert, L., Olivier, M., Romagnan, J.-B., Costa Brandao, M., Lombard, F., Llopis, N.,
482 Courboulès, J., Caray-Counil, L., Serranito, B., Irisson, J.-O., Picheral, M., Gorsky, G., Stemann, L., 2018.
483 ZooScanNet: plankton images captured with the ZooScan. <https://doi.org/10.17882/55741>

484 Feuilletoy, G., Fromentin, J.-M., Saraux, C., Irisson, J.-O., Jalabert, L., Stemmann, L., 2022. Temporal fluctuations
485 in zooplankton size, abundance, and taxonomic composition since 1995 in the North Western Mediterranean Sea.
486 ICES J. Mar. Sci. 79, 882–900. <https://doi.org/10.1093/icesjms/fsab190>

487 Gorsky, G., Ohman, M.D., Picheral, M., Gasparini, S., Stemmann, L., Romagnan, J.-B., Cawood, A., Pesant, S.,
488 Garcia-Comas, C., Prejger, F., 2010. Digital zooplankton image analysis using the ZooScan integrated system. J.
489 Plankton Res. 32, 285–303. <https://doi.org/10.1093/plankt/fbp124>

490 Graham, B., 2014. Spatially-sparse convolutional neural networks. <https://doi.org/10.48550/arXiv.1409.6070>

491 Grandremy, N., Romagnan, J.-B., Dupuy, C., Doray, M., Huret, M., Petitgas, P., 2023a. Hydrology and small
492 pelagic fish drive the spatio-temporal dynamics of springtime zooplankton assemblages over the Bay of Biscay
493 continental shelf. Progress in Oceanography 210, 102949. <https://doi.org/10.1016/j.pocean.2022.102949>

494 Grandremy, N., Dupuy, C., Petitgas, P., Mestre, S.L., Bourriau, P., Nowaczyk, A., Forest, B., Romagnan, J.-B.,
495 2023b. The ZooScan and the ZooCAM zooplankton imaging systems are intercomparable: A benchmark on the
496 Bay of Biscay zooplankton. Limnology and Oceanography: Methods 21, 718–733.
497 <https://doi.org/10.1002/lom3.10577>

498 Grandremy N., Bourriau P., Daché E., Danielou M-M., Doray M., Dupuy C., Huret M., Jalabert L., Le Mestre S.,
499 Nowaczyk A., Petitgas P., Pineau P., Raphalen E., Romagnan J-B., 2023c. PELGAS Bay of Biscay ZooScan
500 zooplankton Dataset (2004-2016). SEANOE. <https://doi.org/10.17882/94052>

501 Grandremy N., Bourriau P., Danielou M-M., Doray M., Dupuy C., Forest B., Huret M., Le Mestre S., Nowaczyk
502 A., Petitgas P., Pineau P., Rouxel J., Tardivel M., Romagnan J-B., 2023d. PELGAS Bay of Biscay ZooCAM
503 zooplankton Dataset (2016-2019). SEANOE. <https://doi.org/10.17882/94040>

504 ICES, 2021. Bay of Biscay and Iberian Coast ecoregion – Fisheries overview (report). ICES Advice: Fisheries
505 Overviews. <https://doi.org/10.17895/ices.advice.9100>

506 Irisson, J.-O., Ayata, S.-D., Lindsay, D.J., Karp-Boss, L., Stemmann, L., 2022. Machine Learning for the Study of
507 Plankton and Marine Snow from Images. Annual Review of Marine Science 14, 277–301.
508 <https://doi.org/10.1146/annurev-marine-041921-013023>

509 Lombard, F., Boss, E., Waite, A.M., Vogt, M., Uitz, J., Stemmann, L., Sosik, H.M., Schulz, J., Romagnan, J.-B.,
510 Picheral, M., Pearلمان, J., Ohman, M.D., Niehoff, B., Möller, K.O., Miloslavich, P., Lara-Lpez, A., Kudela, R.,
511 Lopes, R.M., Kiko, R., Karp-Boss, L., Jaffe, J.S., Iversen, M.H., Irisson, J.-O., Fennel, K., Hauss, H., Guidi, L.,
512 Gorsky, G., Giering, S.L.C., Gaube, P., Gallager, S., Dubelaar, G., Cowen, R.K., Carlotti, F., Briseño-Avena, C.,
513 Berline, L., Benoit-Bird, K., Bax, N., Batten, S., Ayata, S.D., Artigas, L.F., Appeltans, W., 2019. Globally
514 Consistent Quantitative Observations of Planktonic Ecosystems. Front. Mar. Sci. 6.
515 <https://doi.org/10.3389/fmars.2019.00196>

516 Menu, C., Pecquerie, L., Bacher, C., Doray, M., Hattab, T., van der Kooij, J., Huret, M., 2023. Testing the bottom-
517 up hypothesis for the decline in size of anchovy and sardine across European waters through a bioenergetic
518 modeling approach. Progress in Oceanography 210, 102943. <https://doi.org/10.1016/j.pocean.2022.102943>

519 Mitra, A., Castellani, C., Gentleman, W.C., Jonasdottir, S.H., Flynn, K.J., Bode, A., Halsband, C., Kuhn, P.,
520 Licandro, P., Agersted, M.D., Calbet, A., Lindeque, P.K., Koppelman, R., Moller, E.F., Gislason, A., Nielsen,
521 T.G., John, M.S., 2014. Bridging the gap between marine biogeochemical and fisheries sciences; configuring the
522 zooplankton link. *Prog. Oceanogr.* 129, 176–199. <https://doi.org/10.1016/j.pocean.2014.04.025>

523 Mitra, A., Davis, C., 2010. Defining the “to” in end-to-end models. *Prog. Oceanogr.* 84, 39–42.
524 <https://doi.org/10.1016/j.pocean.2009.09.004>

525 Moser, H.G., Ahlstrom, E.H., 1985. Staging anchovy eggs. Southwest Fisheries Center, National Marine Fisheries
526 Service, NOM, PO. Box 271, La Jolla, CA 92038.

527 Ohman, M.D., Romagnan, J.-B., 2016. Nonlinear effects of body size and optical attenuation on Diel Vertical
528 Migration by zooplankton. *Limnology and Oceanography* 61, 765–770. <https://doi.org/10.1002/lno.10251>

529 Orenstein, E.C., Ayata, S.-D., Maps, F., Becker, É.C., Benedetti, F., Biard, T., de Garidel-Thoron, T., Ellen, J.S.,
530 Ferrario, F., Giering, S.L.C., Guy-Haim, T., Hoebeke, L., Iversen, M.H., Kiørboe, T., Lalonde, J.-F., Lana, A.,
531 Laviale, M., Lombard, F., Lorimer, T., Martini, S., Meyer, A., Möller, K.O., Niehoff, B., Ohman, M.D., Pradaliar,
532 C., Romagnan, J.-B., Schröder, S.-M., Sonnet, V., Sosik, H.M., Stemmann, L.S., Stock, M., Terbiyik-Kurt, T.,
533 Valcárcel-Pérez, N., Vilgrain, L., Wacquet, G., Waite, A.M., Irisson, J.-O., 2022. Machine learning techniques to
534 characterize functional traits of plankton from image data. *Limnology and Oceanography* 67, 1647–1669.
535 <https://doi.org/10.1002/lno.12101>

536 Panaiotis, T., Caray-Counil, L., Woodward, B., Schmid, M.S., Daprano, D., Tsai, S.T., Sullivan, C.M., Cowen,
537 R.K., Irisson, J.-O., 2022. Content-Aware Segmentation of Objects Spanning a Large Size Range: Application to
538 Plankton Images. *Frontiers in Marine Science* 9.

539 Petitgas, P., Goarant, A., Masse, J., and Bourriau, P., 2009. Combining acoustic and CUFES data for the quality
540 control of fish-stock survey estimates. *ICES Journal of Marine Science*, 66: 1384–1390.
541 <https://doi.org/10.1093/icesjms/fsp007>

542 Petitgas, P., Doray, M., Huret, M., Masse, J., and Woillez, M., 2014. Modelling the variability in fish spatial
543 distributions over time with empirical orthogonal functions: anchovy in the Bay of Biscay. *ICES Journal of Marine*
544 *Science*, 71: 2379–2389. <https://doi.org/10.1093/icesjms/fsu111>

545 Picheral, M., Colin, S., Irisson, J.O., 2017. EcoTaxa, a tool for the taxonomic classification of images. URL
546 <https://ecotaxa.obs-vlfr.fr/>

547 Queiros, Q., Fromentin, J.-M., Gasset, E., Dutto, G., Huiban, C., Metral, L., Leclerc, L., Schull, Q., McKenzie,
548 D.J., Saraux, C., 2019. Food in the Sea: Size Also Matters for Pelagic Fish. *Frontiers in Marine Science* 6.
549 <https://doi.org/10.3389/fmars.2019.00385>

550 Romagnan, J.B., Aldamman, L., Gasparini, S., Nival, P., Aubert, A., Jamet, J.L., Stemmann, L., 2016. High
551 frequency mesozooplankton monitoring: Can imaging systems and automated sample analysis help us describe
552 and interpret changes in zooplankton community composition and size structure - An example from a coastal site.
553 *Journal of Marine Systems* 162, 18–28. <https://doi.org/10.1016/j.jmarsys.2016.03.013>

554 Saraux, C., Beveren, E.V., Brosset, P., Queiros, Q., Bourdeix, J.-H., Dutto, G., Gasset, E., Jac, C., Bonhommeau,
555 S., Fromentin, J.-M., 2019. Small pelagic fish dynamics: A review of mechanisms in the Gulf of Lions. *Deep Sea*
556 *Research Part II: Topical Studies in Oceanography* 159, 52–61. <https://doi.org/10.1016/j.dsr2.2018.02.010>

557 Sieburth, J., Smetacek, V., Lenz, J., 1978. Pelagic Ecosystem Structure - Heterotrophic Compartments of Plankton
558 and Their Relationship to Plankton Size Fractions - Comment. *Limnol. Oceanogr.* 23, 1256–1263.
559 <https://doi.org/10.4319/lo.1978.23.6.1256>

560 Siegel, D.A., Buesseler, K.O., Behrenfeld, M.J., Benitez-Nelson, C.R., Boss, E., Brzezinski, M.A., Burd, A.,
561 Carlson, C.A., D’Asaro, E.A., Doney, S.C., Perry, M.J., Stanley, R.H.R., Steinberg, D.K., 2016. Prediction of the
562 Export and Fate of Global Ocean Net Primary Production: The EXPORTS Science Plan. *Frontiers in Marine*
563 *Science* 3. <https://doi.org/10.3389/fmars.2016.00022>

564 Steinberg, D.K., Carlson, C.A., Bates, N.R., Goldthwait, S.A., Madin, L.P., Michaels, A.F., 2000. Zooplankton
565 vertical migration and the active transport of dissolved organic and inorganic carbon in the Sargasso Sea. *Deep*
566 *Sea Research Part I: Oceanographic Research Papers* 47, 137–158. [https://doi.org/10.1016/S0967-0637\(99\)00052-](https://doi.org/10.1016/S0967-0637(99)00052-7)
567 [7](https://doi.org/10.1016/S0967-0637(99)00052-7)

568 Turner, J.T., 2015. Zooplankton fecal pellets, marine snow, phytodetritus and the ocean’s biological pump.
569 *Progress in Oceanography* 130, 205–248. <https://doi.org/10.1016/j.pocean.2014.08.005>

570 Uitz, J., Claustre, H., Gentili, B., Stramski, D., 2010. Phytoplankton class-specific primary production in the
571 world’s oceans: Seasonal and interannual variability from satellite observations. *Global Biogeochemical Cycles*
572 24. <https://doi.org/10.1029/2009GB003680>

573 Van Beveren, E., Bonhommeau, S., Fromentin, J.-M., Bigot, J.-L., Bourdeix, J.-H., Brosset, P., Roos, D., Saraux,
574 C., 2014. Rapid changes in growth, condition, size and age of small pelagic fish in the Mediterranean. *Mar Biol*
575 161, 1809–1822. <https://doi.org/10.1007/s00227-014-2463-1>

576 van der Lingen, C., Hutchings, L., Field, J., 2006. Comparative trophodynamics of anchovy *Engraulis encrasicolus*
577 and sardine *Sardinops sagax* in the southern Benguela: are species alternations between small pelagic fish
578 trophodynamically mediated? *African Journal of Marine Science* 28, 465–477.
579 <https://doi.org/10.2989/18142320609504199>

580 Vandromme, P., Nogueira, E., Huret, M., Lopez-Urrutia, A., Gonzalez-Nuevo Gonzalez, G., Sourisseau, M.,
581 Petitgas, P., 2014. Springtime zooplankton size structure over the continental shelf of the Bay of Biscay. *Ocean*
582 *Sci.* 10, 821–835. <https://doi.org/10.5194/os-10-821-2014>

583 Vandromme, P., Stemmann, L., Garcia-Comas, C., Berline, L., Sun, X., Gorsky, G., 2012. Assessing biases in
584 computing size spectra of automatically classified zooplankton from imaging systems: A case study with the
585 ZooScan integrated system. *Methods in Oceanography* 1–2, 3–21. <https://doi.org/10.1016/j.mio.2012.06.001>

586 Véron, M., Duhamel, E., Bertignac, M., Pawlowski, L., Huret, M., 2020. Major changes in sardine growth and
587 body condition in the Bay of Biscay between 2003 and 2016: Temporal trends and drivers. *Progress in*
588 *Oceanography* 182, 102274. <https://doi.org/10.1016/j.pocean.2020.102274>

589 **Appendix A**

590 Table A1: ZooCAM dataset columns header – definition of data and metadata fields.

| Column name | Definition |
|----------------------------|--|
| object_id | name of object and associated image |
| objid | unique ecotaxa internal object identifier |
| object_lat | latitude of sampling |
| object_lon | longitude of sampling |
| object_date | date of sampling |
| object_time | time of sampling |
| object_depth_min | minimum sampling depth |
| object_depth_max | maximum sampling depth |
| object_taxon | taxonomic name |
| object_lineage | full taxonomic lineage corresponding to the taxon |
| classif_id | unique ecotaxa internal taxon identifier |
| object_area | object's surface |
| object_area_exc | object surface excluding white pixels |
| object_%area | proportion of the image corresponding to the object |
| object_area_based_diameter | object's Area Based Diameter: $2 * (\text{object_area}/\pi)^{(1/2)}$ |
| object_meangreyimage | mean image grey level |
| object_meangreyobjct | mean object grey level |
| object_modegreyobjct | modal object grey level |
| object_sigmagrey | object grey level standard deviation |
| object_mingrey | minimum object grey level |
| object_maxgrey | maximum object grey level |
| object_sumgrey | object grey level integrated density: $\text{object_mean} * \text{object_area}$ |
| object_breadth | breadth of the object along the best fitting ellipsoid minor axis |
| object_length | breadth of the object along the best fitting ellipsoid major axis |
| object_elongation | elongation index: $\text{object_length}/\text{object_breadth}$ |
| object_perim | object's perimeter |
| object_minferetdiam | minimum object's feret diameter |
| object_maxferetdiam | maximum object's feret diameter |
| object_meanferetdiam | average object's feret diameter |
| object_feretelongation | elongation index: $\text{object_maxferetdiam}/\text{object_minferetdiam}$ |
| object_compactness | Isoperimetric quotient: the ration of the object's area to the area of a circle having the same perimeter |
| object_intercept0 | the number of times that a transition from background to foreground occurs a the angle 0° for the entire object |

| | |
|-----------------------------|--|
| object_intercept45 | the number of times that a transition from background to foreground occurs at the angle 45° for the entire object |
| object_intercept90 | the number of times that a transition from background to foreground occurs at the angle 90° for the entire object |
| object_intercept135 | the number of times that a transition from background to foreground occurs at the angle 135° for the entire object |
| object_convexhullarea | area of the convex hull of the object |
| object_convexhullfillratio | ratio object_area/convexhullarea |
| object_convexperimeter | perimeter of the convex hull of the object |
| object_n_number_of_runs | number of horizontal strings of consecutive foreground pixels in the object |
| object_n_chained_pixels | number of chained pixels in the object |
| object_n_convex_hull_points | number of summits of the object's convex hull polygon |
| object_n_number_of_holes | number of holes (as closed white pixel area) in the object |
| object_transparence | ratio object_sumgrey/object_area |
| object_roughness | measure of small scale variations of amplitude in the object's grey levels |
| object_rectangularity | ratio of the object's area over its best bounding rectangle's area |
| object_skewness | skewness of the object's grey level distribution |
| object_kurtosis | kurtosis of the object's grey level distribution |
| object_fractal_box | fractal dimension of the object's perimeter |
| object_hist25 | grey level value at quantile 0.25 of the object's grey levels normalized cumulative histogram |
| object_hist50 | grey level value at quantile 0.5 of the object's grey levels normalized cumulative histogram |
| object_hist75 | grey level value at quantile 0.75 of the object's grey levels normalized cumulative histogram |
| object_valhist25 | sum of grey levels at quantile 0.25 of the object's grey levels normalized cumulative histogram |
| object_valhist50 | sum of grey levels at quantile 0.5 of the object's grey levels normalized cumulative histogram |
| object_valhist75 | sum of grey levels at quantile 0.75 of the object's grey levels normalized cumulative histogram |
| object_nobj25 | number of objects after thresholding at the object_valhist25 grey level |
| object_nobj50 | number of objects after thresholding at the object_valhist50 grey level |
| object_nobj75 | number of objects after thresholding at the object_valhist75 grey level |
| object_symetrie_h | index of horizontal symmetry |
| object_symetrie_v | index of vertical symmetry |
| object_thick_r | maximum object's thickness/mean object's thickness |
| object_cdist | distance between the mass and the grey level object's centroids |
| object_bord | tag for object touching the frame edge |

| | |
|--|--|
| sample_id | name of the sample from the object originate |
| sample_ship | name of the ship used to collect the samples |
| sample_campaign | name of the cruise where samples were collected |
| sample_station | name of the station where samples were collected |
| sample_depth | bottom depth at station |
| sample_device | net used to collect the sample |
| sample_fishingvolume | seawater volume sampled |
| sample_sub_part | subsampling elevation factor |
| process_id | name of software/software version used to analysed digitized sample images |
| process_resolution_camera_ micron_par_pixel | pixel size |

591

592 Table A2: ZooScan dataset columns header – definition of data and metadata fields

| Column name | Definition |
|------------------|--|
| object_id | name of object and associated image |
| objid | unique ecotaxa internal object identifier |
| object_lat | latitude of sampling |
| object_lon | longitude of sampling |
| object_date | date of sampling |
| object_time | time of sampling |
| object_depth_min | minimum sampling depth |
| object_depth_max | maximum sampling depth |
| object_taxon | taxonomic name |
| object_lineage | full taxonomic lineage corresponding to the taxon |
| classif_id | unique ecotaxa internal taxon identifier |
| object_area | object's surface |
| object_mean | mean object grey level |
| object_stddev | object grey level standard deviation |
| object_mode | modal object grey level |
| object_min | minimum object grey level |
| object_max | maximum object grey level |
| object_perim. | object's perimeter |
| object_major | length of major axis of best fitting ellipse |
| object_minor | length of minor axis of best fitting ellipse |
| object_circ. | circularity: $4 * \pi (\text{object_area} / \text{object_perim.}^2)$ |
| object_feret | maximum feret diameter |
| object_intden | object grey level integrated density: $\text{object_mean} * \text{object_area}$ |
| object_median | median object grey level |
| object_skew | skewness of the object's grey level distribution |
| object_kurt | kurtosis of the object's grey level distribution |
| object_%area | proportion of the image corresponding to the object |
| object_area_exc | object surface excluding white pixels |
| object_fractal | fractal dimension of the object's perimeter |
| object_skelarea | surface of the one-pixel wide skeleton of the object |
| object_slope | slope of the cumulated histogram of the object grey levels |
| object_histcum1 | the number of times that a transition from background to foreground occurs at the angle 0° |
| object_histcum2 | grey level at quantiles 0.5 of the histogram of the object grey levels |
| object_histcum3 | grey level at quantiles 0.75 of the histogram of the object grey levels |
| object_nb1 | number of objects after thresholding at the object_histcum1 grey level |
| object_nb2 | number of objects after thresholding at the object_histcum2 grey level |

| | |
|--------------------------------|---|
| object_symetrieih | index of horizontal symmetry |
| object_symetrieiv | index of vertical symmetry |
| object_symetrieihc | index of horizontal symmetry after thresholding at the object_histcum1 grey level |
| object_symetrieivc | index of vertical symmetry after thresholding at the object_histcum1 grey level |
| object_convperim | perimeter of the convex hull of the object |
| object_convarea | area of the convex hull of the object |
| object_fcons | object's contrast |
| object_thickr | maximum object's thickness/mean object's thickness |
| object_esd | object's Equivalent Spherical Diameter: $2 * (\text{object_area}/\pi)^{(1/2)}$ |
| object_elongation | elongation index: major/minor |
| object_range | range of greys: max-min |
| object_meanpos | relative position of the mean grey: (max-mean)/range |
| object_centroids | distance between the mass and the grey level object's centroids |
| object_cv | coefficient of variation of greys: $100 * (\text{stddev}/\text{mean})$ |
| object_sr | index of variation of greys: $100 * (\text{stddev}/\text{range})$ |
| object_perimareaexc | index of the relative complexity of the perimeter: $\text{object_perim}/\text{object_area_exc}$ |
| object_feretareaexc | another elongation index : $\text{object_feret}/\text{object_area_exc}$ |
| object_perimferet | index of the relative complexity of the perimeter: $\text{object_perim}/\text{object_feret}$ |
| object_perimmajor | index of the relative complexity of the perimeter: $\text{object_perim}/\text{object_major}$ |
| object_circexc | circularity of object excluding white pixels: $4 * \pi * (\text{object_area_exc}/\text{object_perim})^2$ |
| object_cdexc | distance between the mass and the grey level object's centroids calculated with object_area_exc |
| sample_id | name of the sample from the object originate |
| sample_ship | name of the ship used to collect the samples |
| sample_program | name of the cruise where samples were collected |
| sample_stationid | name of the station where samples were collected |
| sample_bottomdepth | bottom depth at station |
| sample_net_type | net used to collect the sample |
| sample_tot_vol | seawater volume sampled |
| sample_comment | comments associated with sampling/sample treatment |
| process_id | name of software/software version used to analysed digitized sample images |
| process_particle_pixel_size_mm | pixel size |
| acq_id | name of subsample if any |
| acq_min_mesh | minimum sieve size of subsample |
| acq_max_mesh | maximum sieve size of subsample |
| acq_sub_part | subsampling elevation factor |

593

594